Computational Insights into the Chemical Structures and Mechanisms of the Chromogenic and Neurotoxic Effects of Aromatic γ-diketones

Chang-Guo Zhan,[†] Peter Spencer,[‡] and David A. Dixon*[,†]

Theory, Modeling & Simulation, William R. Wiley Environmental Molecular Sciences Laboratory, Pacific Northwest National Laboratory, MS K1-83, P.O. Box 999, Richland, Washington 99352, and Center for Research on Occupational and Environmental Toxicology, Oregon Health Sciences University, 3181 Southwest Sam Jackson Park Road L606, Portland, Oregon 97201

Received: September 26, 2002; In Final Form: January 9, 2003

The chromogenic properties of various candidate structures, i.e., isoindole monomers and dimers and their derivatives, of the chromophores formed from the reactions of 1,2-diacetylbenzene (1,2-DAB), a typical representative of chromogenic and neurotoxic aromatic γ-diketones, with NH_3, amino acids, and proteins, have been calculated by using density functional theory. The calculated results indicate that the isoindole monomers should not exhibit a color, whereas the isoindole derivative dimers should all be colored. Further oxidization of the isoindole derivative dimers can significantly change the colors of the dimers, and the results calculated for the oxidized isoindole derivative dimers are completely consistent with all of the experimental data for the chromogenic and neurotoxic effects of 1,2-DAB. It has been demonstrated that the violet/blue chromophores formed from the reactions of 1,2-DAB with amino acids/proteins under neutral and acidic conditions are likely to be the oxidized isoindole derivative dimer structures (like **7b)** cross-linking the proteins, whereas the brown chromophores formed when pH ≥ 7.5 could be the oxidized dimer structures (like **7a**) without cross-linking proteins. Our results strongly support the conclusion that the chromogenic effects of aromatic γ-diketones are closely related to their neurotoxic effects and further predict that both the chromogenic and neurotoxic effects are associated with the same chemical reaction process under the neutral and acidic conditions. Such a reaction process most likely starts from the formation of the isoindole−protein adducts followed by the dimerization and further oxidization.

Introduction

A variety of aromatic neurotoxic organic solvents produce chromogenic effects in humans and animals through their oxidation metabolites, aromatic γ-diketones. Aromatic hydrocarbon compounds that can lead to chromogenic/neurotoxic behavior are present in fuels and solvents and, formerly, in consumer products; they also occur in contaminated soil and water at hazardous-waste sites.[1] The fact that certain aromatic hydrocarbons exhibit chromogenic and neurotoxic behavior has been known for a number of years where a chromogenic species is defined as one that is colored and can be observed. For example, in 1979, Spencer et al.[2] described the remarkable chromogenic and neurotoxic effects of acetyl ethyl tetramethyl tetralin (AETT), a fragrance raw material and food additive that was subsequently removed from consumer products.[3]

The oxidation metabolites of chromogenic aromatic hydrocarbon compounds, the aromatic γ-diketones, have a common 1,2-diacetyl moiety, display similar chromogenic properties, and induce neuropathological changes in the rodent central and peripheral nervous system.[3] However, the parent diketones are colorless. As one of the simplest representatives of the chromogenic and neurotoxic aromatic hydrocarbon compounds, 1,2-diethylbenzene (1,2-DEB) and its oxidation metabolite 1,2-diacetylbenzene (1,2-DAB**, 1a** in Scheme 1) have drawn great attention.[3−9] They form blue pigments on contact with proteins, skin, and other tissues.[3,7] Rodents treated systemically with 1,2-DEB or 1,2-DAB develop blue discoloration of skin, eyes, and internal organs, including the brain and spinal cord.[4−7,10] The color of the formed pigment is pH-dependent; the pigment displays a blue or violet color in neutral and acidic solutions, and it exhibits a brown color at pH ≥ 7.5.[7,9] On the basis of the available experimental data, it has been hypothesized that the chromogenic and neurotoxic properties of 1,2-DAB are strongly correlated to their reactions with amino acids containing a primary amino group.[6,7] In particular, lysine exhibits the highest reactivity.[7,9] Thus, knowledge about the mechanism of the chromogenic effects could provide valuable insights into the fundamental mechanism of the neurotoxicity. Mechanistic understanding of both chromogenic and neurotoxic effects could lead to the development of biomarkers of exposure to these neurotoxic compounds.

A number of experimental studies have provided insights into the molecular mechanism of the chromogenic effects of 1,2-DAB and related species. Previously reported experimental results and structure−activity considerations pointed to two possibilities suggested in the literature.[6] First, the chromogenicity was proposed to result from the formation of a ninhydrin-like compound that reacts with proteins to generate a colored pigment,[3] i.e., Ruhemann's purple (the chromophore). The other hypothesis is that 1,2-DAB reacts with the ε amino groups of lysine in a manner equivalent to that of the neurotoxic aliphatic γ-diketones (such as 2,5-hexanedione, 2,5-HD, the active metabolite of the solvent *n*-hexane) that form 2,5-dimethylpyrrole adducts with proteins, including neurofilament peptides.[11] According to this hypothesis, the chromophore responsible for

[†] Pacific Northwest National Laboratory.
[‡] Oregon Health Sciences University.

10.1021/jp0221486 CCC: $25.00
Published on Web 03/05/2003

SCHEME 1

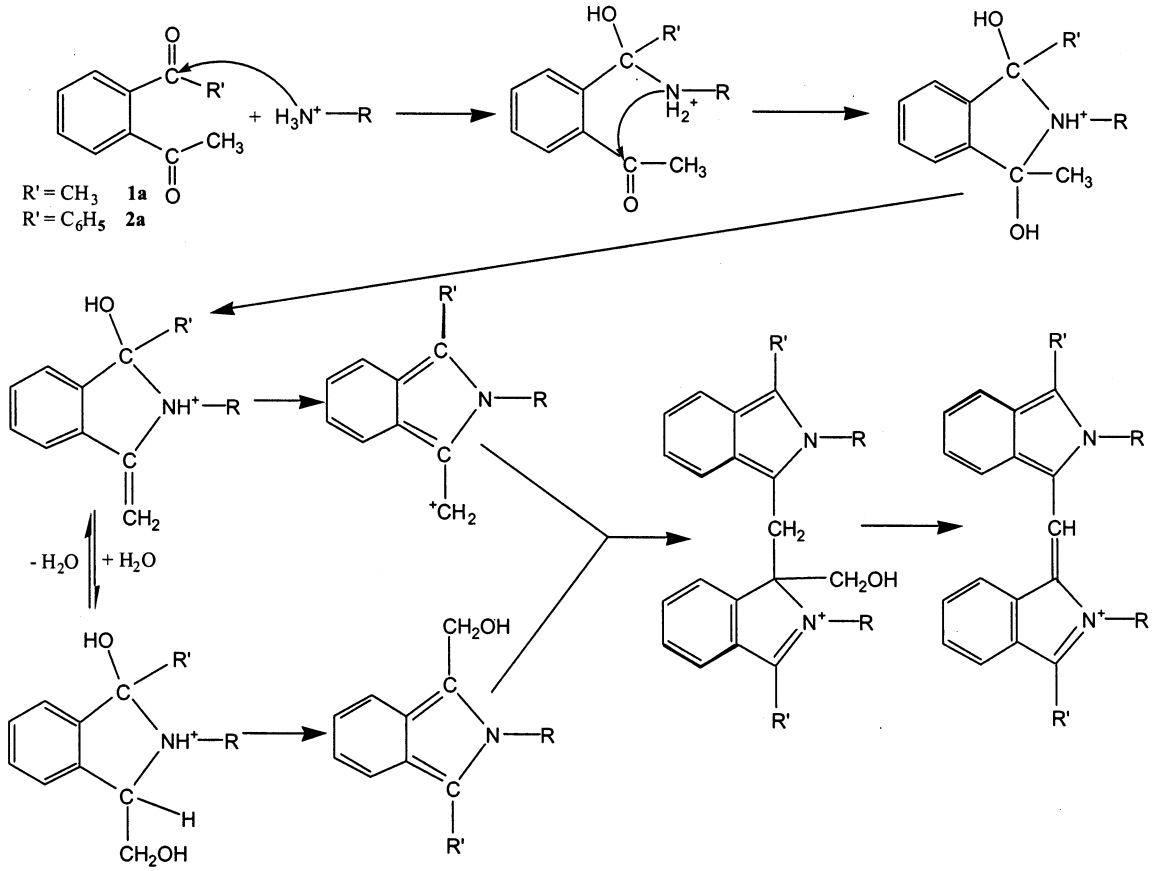

the chromogenic effects of 1,2-DAB should be a pyrrole-like adduct. The former hypothesis is supported by well-established chemistry[12] of the ninhydrin color test leading to a blue color. The latter hypothesis is supported by the experimental demonstration that 1,2-DAB induces 2,5-HD-like giant axonal swellings filled with neurofilaments.[10] It is difficult to identify the chromophores by experiment alone because the reaction systems are all complicated mixtures and the reaction products have not been separated yet. Therefore, the reliable theoretical prediction of possible chromophores is needed to complement ongoing experimental investigations to uncover the molecular mechanism of the chromogenic effects.

There have been dramatic changes in computational chemistry over the last two decades. Electronic structure theory has become an effective and powerful tool for use in predicting the properties of a wide range of molecules including geometries, energetics and spectroscopic (IR/Raman vibrational spectra, NMR, and UV−vis). One of the main reasons for the acceleration of the use of electronic structure theory in predicting molecular properties for larger molecules has been the development of density functional theory (DFT).[13−15] The combination of low computational cost with reasonable accuracy has led to the successful application of the DFT method to the prediction of a broad range of properties of molecules in the ground state.[16] In contrast to the case of ground states, time-dependent density functional theory (TD-DFT) for treating excited-state properties[17−19] has only recently been applied to molecules,[20,21] although the theory itself was first proposed more than 20 years ago. Recent work has shown that TD-DFT can be used to reliably predict not only the location of the UV−vis excitation but also the oscillator strength (intensity of the transition).[22,23] In addition, Adamo and Barone[24] have tested TD-DFT calculations in aqueous solution; their calculated results indicate that the solvent shifts of the calculated excitation energies are small compared to the accuracy required to qualitatively predict the color of a compound.

Our long-term goal is to establish a firm structural and mechanistic understanding of both the chromogenic and neurotoxic effects of γ-diketones through an extensive, coupled experimental/computational effect. Significant work has already been done on these systems for many years but due to the complexity of the problem, no final answer is yet available. This work is meant to contribute in part to the solution of the problem. As part of a combined experimental/computational study focused on uncovering the molecular mechanism of the chromogenic and neurotoxic effects of aromatic neurotoxicants, we recently reported the first computational study on the chromogenic effects of aromatic neurotoxicants to theoretically examine the above-mentioned two hypotheses for the possible chromophores.[8] A series of ab initio and DFT calculations were performed on two representative aromatic compounds, 1,2-DAB and 1,2-diacetyl tetramethyl tetralin (1,2-DATT), the putative active metabolites of 1,2-DEB and AETT, and on the products of their possible reactions with proteins that result in chromogenic effects. The electronic excitation energies determined by different computational approaches were found to be consistent with each other. The calculated results consistently indicated that only products of ninhydrin-like reactions have the expected blue color, whereas the hypothesized pyrrole-like compounds themselves do not display a color.[8] Thus, the hypothesized pyrrole-like compounds themselves can be excluded. The chromogenic effects of 1,2-DAB (or 1,2-DEB) and 1,2-DATT (or AETT) could only result from either ninhydrin-like reactions or other unknown types of compounds.

To test our calculated results and the resulting mechanistic hypothesis rats were treated directly with ninhydrin, and the

SCHEME 2

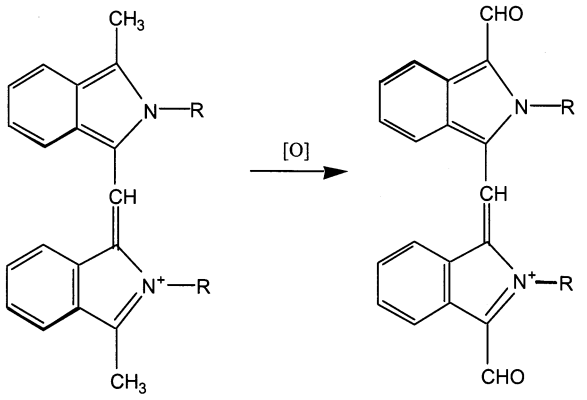

ninhydrin-treated animals indeed showed at the injection site a blue discoloration of skin.[7] However, no discoloration of internal organs was seen and ninhydrin lacks systemic neurotoxicity as compared to 1,2-DAB. Further experimental studies were performed to identify the amino acid and protein targets of 1,2-DAB and ninhydrin by assessing their differential reactivity with neural and nonneural amino acids and proteins in vitro and in vivo.[9] It has been shown that the neurotoxic mechanisms of aromatic γ-diketones are similar to those of aliphatic γ-diketones; they are all related to neurofilaments, which are composed of cytoskeletal triplet proteins that move anterogradely from their site of synthesis in the nerve cell body along the axon to the nerve terminal. Neurofilament transport is also blocked by systemic treatment with the aromatic γ-diketones, which cross-link neurofilament proteins to form higher-molecular-weight products. The cross-linked neurofilaments are unable to move anterogradely along the axon. Whereas 1,2-DAB can cross-link neurofilament proteins to produce the higher-molecular-weight products, ninhydrin forms a chromophore without evidence of the intermolecular protein−protein cross-linking.[9]

The integrated results of the joint computational[8] and experimental[7,9] studies led to a deeper insight into the molecular mechanism of chromogenic and neurotoxic effects of the aromatic neurotoxicants and imply that the chromophores in the chromogenic effects of the aromatic neurotoxicants could be neither the pyrrole-like compounds nor the products of ninhydrin-like reactions. Some other molecular structures could also contribute to the observed blue discoloration, although it cannot be ruled out that the products of ninhydrin-like reactions are present as the chromophores due to varying in vivo diffusion and reaction processes.[7] Thus, it is necessary to explore new candidates of the chromophores to design new experiments.

In the present study, we have further employed first-principles electronic structure methods, including DFT and recently developed fully polarizable continuum solvation theory,[25] to predict the structures, energetics, and colors of various new chromophore candidates hypothesized in light of the latest results.[7,9] The calculated spectral and thermodynamic properties of two kinds of oxidized isoindole derivative dimers are completely consistent with all of the experimental results for the chromogenic and neurotoxic effects of 1,2-DAB. On the basis of the calculated results, the formation of the oxidized dimer of isoindole derivatives (Schemes 1 and 2) not only can explain the observed blue/violet discoloration and protein cross-linking under the physiological condition but also can explain the observed pH dependence of the colored pigment, suggesting that both the chromogenic and neurotoxic effects of the aromatic neurotoxicant follow the same molecular mechanism to form the oxidized isoindole derivative dimers.

Computational Details

Geometries of all species considered in this study were fully optimized by using gradient corrected-DFT with Becke's three-parameter hybrid exchange functional and the Lee−Yang−Parr correlation functional (B3LYP)[26] and the 6-31G(d) basis set.[27] Analytical second derivative calculations, which yield the harmonic vibrational frequencies, were performed at the optimized geometries to ensure that the optimized geometries are minima on the potential energy hypersurface (all real frequencies). The geometries optimized at the B3LYP/6-31G(d) level were further refined at the B3LYP/6-31+G(d) level of theory. Our previous computational studies indicate that for the purpose of investigation on the products of the aromatic γ-diketone reactions with amino acids, the geometry optimizations at the B3LYP/6-31G(d) and B3LYP/6-31+G(d) levels are sufficient; the use of larger basis sets should not significantly change the finally calculated energetic and spectral results. Hence, the geometries optimized at the B3LYP/6-31+G(d) level were used in the calculation of the energies of the singlet vertical excited states to evaluate the UV−vis spectrum by using time-dependent DFT (i.e., TD-DFT)[28] with the B3LYP functional and the 6-31G(d) basis set augmented with a set of Rydberg functions (3s3p3d) centered at the molecular mass center (mc).[29] The Gaussian exponents of this set of Rydberg functions are 0.005858 (3s), 0.003346 (4s), 0.002048 (5s), 0.009988 (3p), 0.005689 (4p), 0.003476 (5p), 0.014204 (3d), 0.008077 (4d), and 0.004927 (5d). This set of Rydberg functions has been used in recently reported calculations of the electronic excitations in pyrrole.[29,30] For convenience, this extended basis set is denoted by 6-31G(d)+Ryd(mc). In addition, larger basis sets, including 6-31++G(d,p), 6-311++G(d,p), 6-311++G(2d,2p), 6-311++G(2df,2pd), and 6-311++G(3df,3pd) and aug-cc-pVDZ and aug-cc-pVTZ,[31] were also used in some of the energy calculations (see below). All of the TD-DFT calculations were performed in the gas phase.

To estimate the thermodynamic equilibration between the two kinds of isoindole derivative dimers, for two species (**3a** and **3b**), the geometries optimized at the B3LYP/6-31+G(d) level in the gas phase were used in self-consistent reaction field (SCRF) calculations at the HF/6-31+G(d) level to calculate the free energies of solvation in aqueous solution. The calculated free energy in solution was taken as the free energy calculated at various levels in the gas phase with the B3LYP/6-31+G(d) zero-point and other vibrational energy corrections plus the solvent shift calculated at the HF/6-31+G(d) level. The present SCRF method was developed and implemented recently in a local version of GAMESS program[32] by one of us, and is called the surface and volume polarizations for electrostatic interaction (SVPE) model.[25] The SVPE model is also known as the fully polarizable continuum model (FPCM)[33−38] because it fully accounts for both surface and volume polarization effects in the SCRF calculation through an efficient three-dimensional integration algorithm.[25a] The current version of the SVPE implementation[25a] has its own limitations. In particular, the analytic energy derivatives required for geometry optimization have not yet been derived and dynamic solvation effects on vertical electronic excitation energies are not included. Therefore, the current SVPE implementation is not capable of performing geometry optimization and there may be errors in the calculated vertical excitation energy in solution. Because the solute cavity surface is defined as a solute electron charge isodensity contour determined self-consistently during the SVPE iteration process, the SVPE results, converged to the exact solution of Poisson's equation with a given numerical tolerance,

SCHEME 3

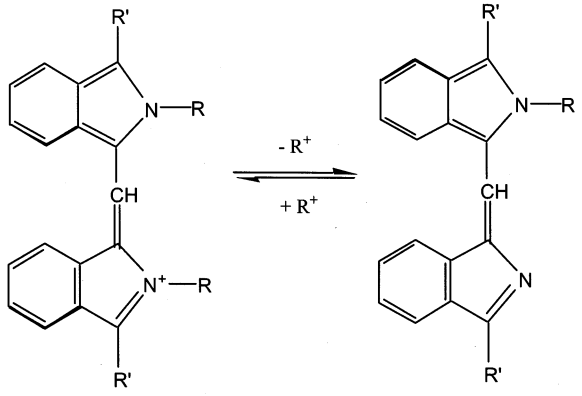

3b	R' = H, R = H	**3a**
4b	R' = C_6H_5, R = H	**4a**
5b	R' = CHO, R = H	**5a**
6b	R' = H, R = CH_3	**6a**
7b	R' = CHO, R = CH_3	**7a**
8b	R' = CH_3, R = CH_3	**8a**

depend only on the contour value at a given dielectric constant and a certain quantum chemical calculation level.[25a] This single parameter value has been determined to be 0.001 au on the basis of an extensive calibration study.[25b] The SVPE procedure using the 0.001 au contour has been shown to be reliable for predicting the free energy of solvation and the pK_a in other biologically interesting systems.[34,36,38c] Previous pK_a calculations[8] on other similar molecules also indicate that using geometries optimized in solution, instead of those in gas phase, does not significantly change the results. The dielectric constant of water used for the solvation calculations is 78.5.

Geometry optimizations and gas-phase energy evaluations were performed by using the Gaussian98 program.[39] A local version[25a] of the GAMESS program[32] was used to perform the SVPE calculations. All calculations were performed on an SGI Origin 2000 computer.

Results and Discussion

Geometries. The molecules considered in this study are shown in Scheme 3. **4a** and **4b** are thought to be the deprotonated and protonated products of the reaction of **2a** with ammonia (NH_3).[40] Similarly, **3a**, **3b**, **5a**, and **5b** are expected to be the products of the reactions of other aromatic γ-diketones with NH_3 (or NH_4^+ for which R = H), as indicated in Scheme 1. The other isoindole derivative dimers all refer to the model structures of possible products of the reactions of aromatic γ-diketones with free amino acids or amino acid residues of proteins as shown in the various Schemes. In our calculations, we only used R = H or CH_3.

All of the stable geometries optimized at the B3LYP/6-31+G(d) level are provided as Supporting Information. The stable structures of the monomers, i.e., **9a**, **10a**, and **11a** (Chart 1) are all planar. The structures of the isoindole derivative dimers also tend to be planar, favoring an extended, conjugated π-bonding system, but only the **3a** and **5a** structures are perfectly planar. Although the framework structures of the other dimers all slightly deviate from planarity due to steric resistance between the bulk groups represented by R and R′, the extended, conjugated π-bonding systems are approximately maintained.

To estimate the thermodynamic equilibration between the deprotonated and protonated states of the products of the reaction of aromatic γ-diketone with NH_3, we calculated the pK_a for

CHART 1

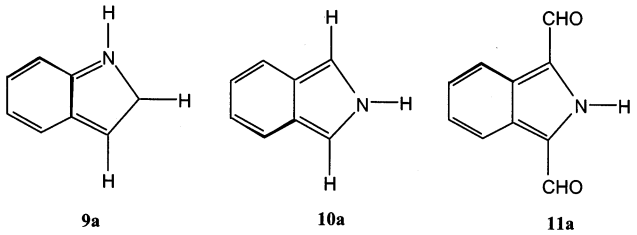

9a **10a** **11a**

the deprotonation process **3b** → **3a** + H^+ by performing a series of first-principles calculations on the gas-phase geometries of **3a** and **3b**, using the DFT method with various basis sets for the gas-phase electronic energy difference and the SVPE-HF/6-31+G(d) method for the solvation energy difference. The value of the SVPE-HF/6-31+G(d) free energy difference for **3a** and **3b** is −44.0 kcal/mol.

It is also necessary for the prediction of the absolute pK_a to know the absolute free energy of the proton in aqueous solution. For the gas-phase proton, accounting for contributions of proton translation to enthalpy and entropy, we have $H(T = 298\ \text{K}) = 1.5$ kcal/mol and $-TS = -7.8$ kcal/mol at $T = 298$ K and pressure of 1 atm.[41] The "experimental" hydration free energy of the proton has a wide range (from −252.6 to −264.1 kcal/mol).[42,43] The largest negative value, −264.1 kcal/mol, is the most recent[44] and is close to recent theoretical values.[37,42] We recently calculated the absolute hydration free energy of the proton, $\Delta G_{hyd}^{298}(H^+)$, by using a high-level, ab initio method incorporating a hybrid supermolecule-continuum approach based on the same SVPE procedure used in the present study. $\Delta G_{hyd}^{298}(H^+)$ was accurately predicted to be −262.4 kcal/mol.[37] Although it has not been possible to isolate one type of ion and measure its absolute hydration free energy by experiment, direct experimental thermodynamic data for different pairs of ions can lead to relative magnitudes of the ionic hydration free energies. The high accuracy of the predicted absolute hydration free energy of proton has been confirmed by applying the same computational protocol to predict the absolute hydration free energy of Li^+: $\Delta G_{hyd}^{298}(Li^+) = -125.1$ kcal/mol, which is larger than $\Delta G_{hyd}^{298}(H^+)$ by 137.3 kcal/mol.[37] The calculated hydration free energy change for solvation of a proton to solvation of Li^+ is 137.5 kcal/mol from the latest collection of experimental data[44] and 137.0 kcal/mol from the earlier experimental data.[43] Our theoretical value is between the two experimental values. With the same approach, the $\Delta G_{hyd}^{298}(HO^-)$ value is accurately predicted to be −104.5 kcal/mol.[38a] The predicted $\Delta G_{hyd}^{298}(HO^-)$ and $\Delta G_{hyd}^{298}(H^+)$ values allow the prediction of the sum of absolute hydration free energies of the proton and hydroxide to be −366.9 kcal/mol, in excellent agreement with the experimental thermodynamic values of -367.1 ± 0.2 kcal/mol (based on NIST gas-phase experimental value[44,45]) and -366.6 ± 0.1 kcal/mol (based on a very recently revised gas-phase experimental value[46]).

The total free energy of solvation for the deprotonation process **3b** → **3a** + H^+ is calculated to be −218.4 kcal/mol. The pK_a is calculated as $\text{p}K_a = \Delta G_{sol}/(2.303RT)$ at $T = 298$ K. The calculated pK_a results as a function of basis set are summarized in Table 1, where different basis sets are arranged in the ordering of their total number of contracted basis functions. There is a significant difference between the B3LYP/6-31+G(d) result and the B3LYP/6-31++G(d,p) result; similar differences have been noted in previously reported studies.[47] In going from the B3LYP/6-31++G(d,p) to the larger basis sets, the changes of the calculated pK_a value are significantly smaller. Our best estimate of the pK_a value calculated using

TABLE 1: Gibbs Free Energy Change (kcal/mol, at 298 K and 1 atm) for 3b → 3a + H^+ and the Corresponding pK_a Calculated with Different Basis Sets[a]

method[b]	no. of BF's[c]	ΔG_{gas}	ΔG_{sol}	pK_a
B3LYP/6-31+G(d)	387	224.9	6.5	4.7
B3LYP/6-31++G(d,p)	439	228.0	8.5	6.2
B3LYP/6-311++G(d,p)	509	226.5	8.1	5.9
B3LYP/aug-cc-pVDZ	554	226.1	7.7	5.7
B3LYP/6-311++G(2d,2p)	643	227.2	8.8	6.4
B3LYP/6-311++G(2df,2pd)	841	227.7	9.2	6.8
B3LYP/6-311++G(3df,3pd)	975	227.6	9.1	6.7
B3LYP/aug-cc-pVTZ	1173	227.5	9.0	6.6

[a] pK_a obtained from single point energy calculations using the geometries optimized at the B3LYP/6-31+G(d) level. [b] Method used for the gas-phase energy calculations. The zero-point vibrational and thermal corrections were calculated at the B3LYP/6-31+G(d) level. The free energies of solvation were determined by performing the FPCM calculations at the HF/6-31+G(d) level. [c] The number of contracted basis functions for the protonated structure.

the largest basis set, i.e., aug-cc-pVTZ, is 6.6. A value of pK_a ≈ 6.6 indicates that when the pH value is about 6.6, the concentrations of the deprotonated and protonated structures should be equal to each other. At lower pH, the protonated structure should be dominant, whereas at higher pH the deprotonated structure should be dominant. We expect that the pK_a values for the deprotonation processes **4b** → **4a** + H^+ and **5b** → **5a** + H^+ should also be close to the pK_a value of ~6 to 7.

Electronic Excitation Energies and Possible Reaction Products under Acidic Condition. On the basis of the optimized geometries, we evaluated the electronic excitation energies by performing TD-DFT calculations at the B3LYP/6-31G(d)+Ryd(mc) level. The calculated first excitation energies (E_{calc}) and the corresponding oscillator strengths (*f*) are summarized in Table 2. For molecules that have more than one absorption in the visible region, the strongest absorption (i.e., the largest *f* value) is associated with the first excitation; the *f* values for the others are all negligible compared to the first one. All of the excitations listed in Table 2 are predicted to be $\pi \rightarrow \pi^*$ transitions.

Our previous computational studies[8] of other molecules, including the products of possible ninhydrin-like reactions of 1,2-DAB and 1,2-DATT with amino acids and proteins, indicate that the excitation energies determined by the TD-DFT calculations are very close to those determined by more sophisticated complete active space multiconfiguration self-consistent field (CASSCF) calculations followed by second-order Møller−Plesset (MP2) perturbations on the multiconfigurational reference states (CAS-MP2).[48] Both the TD-DFT and CAS-MP2 results[8] are in excellent agreement with available experimental data.

The reliability of the TD-DFT results obtained in the present study can further be examined by comparison with available experimental results. The experimental UV−vis spectrum[45] is available for **9a**, showing three absorption bands between 290 and 240 nm. The first absorption band, at ~287 nm (~4.32 eV), is relatively weaker than the other two bands at ~279 nm (~4.44 eV) and ~271 nm (~4.58 eV). There is strong overlap of the peaks in the experimental spectrum so it is hard to determine the exact relative intensities and peak positions. The TD-DFT results predict that the first excitation of **9a** (at ~278 nm) is associated with an oscillator strength of 0.0033 and that between 278 and 240 nm there are only two excitations with greater oscillator strengths, a peak at 257 nm with $f = 0.0725$ and a peak at 249 nm with $f = 0.0329$. To simulate the absorption spectrum of **9a**, each of the calculated transitions (15) between 278 and 229 nm was represented by a Lorentzian distribution with a half-peak width of 0.075 eV. The simulated spectrum in the region of 240 to 290 nm is displayed in Figure 1 and clearly shows three peaks at ~278, ~257, and ~249 nm, which can be correlated with the three peaks at ~287, ~279, and ~271 nm in the experimental UV−vis spectrum.[45] Compared to the experimental UV−vis spectrum,[45] the predicted relative intensity of the first absorption band at ~278 nm is apparently too weak and the relative intensities of the two strong absorption bands are reversed as compared to experiment, suggesting that the theoretical prediction of the absorption intensities is not that accurate. Nevertheless, in both the simulated and experimental spectra, the first absorption band is significantly weaker than the other two absorption bands, suggesting that our correlation of the first absorption band with the first electron excitation for **9a** is correct. The first excitation energy of 4.46 eV (~278 nm) calculated for **9a** differs from

TABLE 2: Calculated First Electronic Excitation Energies (eV and nm) and Oscillator Strengths (*f*) for the Relevant Neutral and Cationic Molecules Obtained From TD-DFT Calculations at the B3LYP/6-31G(d)+Ryd(mc) Level[a]

substituents in dimer		neutral molecule				cationic molecule			
R′	R		eV	nm	f		eV	nm	f
H	H	**3a**	2.82 (2.76)	455	0.8380	**3b**	2.54 (2.41)	489	0.8670
C_6H_5	H	**4a**	2.38 (2.40)	521	0.8825	**4b**	2.19 (2.14)	566	0.9468
CHO	H	**5a**	2.41 (2.33)	515	0.6962	**5b**	2.12 (1.98)	585	0.6622
H	CH_3	**6a**	2.89 (2.85)	430	0.9311	**6b**	2.51 (2.43)	495	0.7824
CHO	CH_3	**7a**	2.45 (2.40)	507	0.7257	**7b**	2.10 (1.99)	589	0.6653
CH_3	CH_3					**8b**	2.51 (2.42)	494	0.9093
		9a	4.46[b] (5.11)	278[b]	0.0033				
		10a	3.82 (4.37)	324	0.0000				
		11a	3.34 (3.43)	371	0.0000				

[a] All excitations are calculated to be $\pi \rightarrow \pi^*$ transitions. The values given in parentheses are the corresponding HOMO−LUMO energy gaps calculated at the B3LYP/6-31G(d)+Ryd(mc) level. [b] The first absorption (i.e., with the longest wavelength) was observed at ~287 nm (~4.32 eV), as shown in the UV−vis spectrum (ref 45).

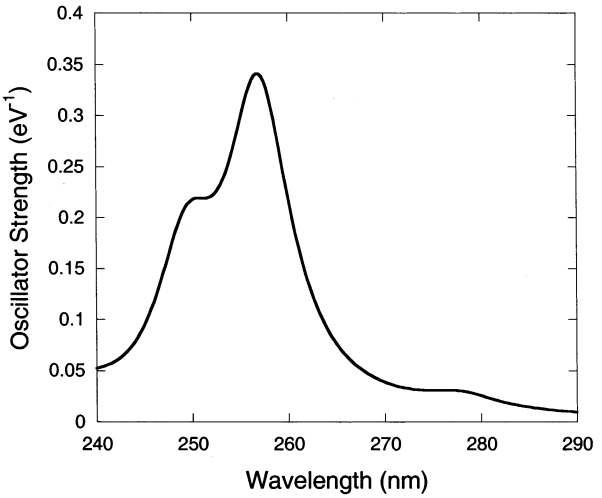

Figure 1. UV−visible spectrum for **9a** calculated at the TD-DFT B3LYP/6-31G(d)+Ryd(mc) level.

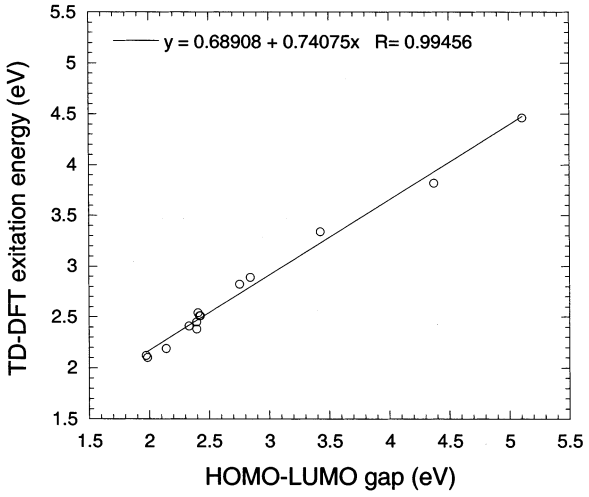

Figure 2. Plot of the first excitation energies obtained from the TD-DFT calculations versus the HOMO−LUMO energy gaps calculated at the B3LYP/6-31G(d)+Ryd(mc) level.

the experimental value by only ∼0.14 eV (∼9 nm). The second peak and first intense absorption, 4.82 eV (∼257 nm), is calculated to be lower than the experimental value by ∼0.4 eV (∼20 nm) and the third peak and second intense absorption, 4.97 eV (∼249 nm) is calculated to be lower than the experimental value by ∼0.39 eV (∼22 nm). These results are consistent with our previous finding[49] in a theoretical study of the photoelectron spectra of pyrrole that the TD-DFT results are less accurate for higher lying excited states than those for the low-lying excited states. We note that the focus of the present study is first excitation energies where the method does indeed do better. This suggests that the TD-DFT results should be providing reliable estimates of the first excitation energies for these molecules; the TD-DFT calculations only slightly overestimate the first excitation energies, e.g., only slightly underestimate the wavelengths of the corresponding absorptions. This is consistent with the reported experimental observation of the blue color for **4b**, a known product of the reaction of **2a** with NH_3 under acidic condition. As observed by Maekawa and Nan'Ya et al.[40] and expected from our estimated pK_a value of 6.6 for the similar isoindole derivative dimers, the product of the reaction of **2a** with NH_3 under acidic condition is dominated by the protonated structure **4b**, rather than the deprotonated structure **4a**. **4b** has the strongest absorption at ∼566 nm, or at a slightly longer wavelength with the consideration of a possible 0.14 eV overestimation of the excitation energy as seen for **9a**. It means that the color of the main light absorbed by **4b** should be close to yellow (∼580 nm) or orange (∼620 nm).[50] Because the complementary color of yellow/orange is violet/blue,[51] the corresponding color of the nonabsorbed light should be close to violet or blue.

We considered whether the model compounds, i.e., with the simplified R structures, used in our practical computations are too simplified to represent the corresponding real structures of the products for the reactions with amino acids or proteins for the purpose of determination of their electronic absorptions. Previous computational studies[8] of the adducts (similar to **10a**) between lysine (denoted by $R-NH_3^+$ here) and the pyrrole-like compounds indicate that the calculated first excitation energy has little change (<∼0.14 eV) when the remaining part of lysine (i.e., R) is simplified to be CH_3. As shown in Table 2, all of the structural changes from R = H to R = CH_3 do not significantly change the predicted absorptions for both neutral and cationic molecules. The calculated absorptions are not very sensitive to the structural changes of these saturated substituents that have no direct contribution to the conjugated π-bonding. So, the isoindole monomer, **10a** or its protonated form, can be considered to be a reasonable model structure of the direct product/intermediate for the reaction of **1a** for amino acids/proteins, and **3b**, **6b**, and **8b** all can be regarded as reasonable model structures of the direct products of the possible dimerization of the isoindole derivatives formed under acidic condition.

According to the TD-DFT results summarized in Table 2, the calculated first excitation energy (due to the $\pi \rightarrow \pi^*$ transition) decreases and the corresponding wavelength of the absorption increases with increasing the size of the conjugated π-bonding system. This is because the HOMO−LUMO energy gap ($\Delta\epsilon_{HL}$) usually becomes smaller when the size of the conjugated π-bonding system increases. As shown in Table 2, the directly calculated HOMO−LUMO energy gaps (at the B3LYP/6-31G(d)+Ryd(mc) level, without any empirical correction) are very close to the excitation energies determined by the TD-DFT calculations, particularly for the dimer structures. The difference between the calculated $\Delta\epsilon_{HL}$ values and the excitation energies (E_{calc}) is dependent on the magnitude of the E_{calc} or $\Delta\epsilon_{HL}$ value. The larger the E_{calc} (or $\Delta\epsilon_{HL}$) value, the larger the difference.

We have recently demonstrated good linear correlation relationships between the DFT HOMO and LUMO energies and certain molecular properties, including ionization potential, electron affinity, electronegativity, hardness, and first electron excitation energy.[52] In particular, a good linear correlation exists between the calculated HOMO−LUMO energy gaps and the first excitation energies.[52] Now we examine whether this kind of linear correlation exists in the biologically interesting molecules considered in the present study. There is, in fact, an excellent linear correlation relationship between the calculated $\Delta\epsilon_{HL}$ values and first excitation energies (E_{calc})

$$E_{calc} = 0.741(\Delta\epsilon_{HL}) + 0.689 \text{ eV} \quad (1)$$

with a root-mean-square deviation (RMSD) of ∼0.069 eV and a correlation coefficient (R) of ∼0.995. This correlation is depicted in Figure 2. It follows that the first excitation energies of the molecules can be roughly estimated from the calculated HOMO−LUMO energy gaps, which can be very useful in future computational studies of molecular chromogenic properties. In addition, the linear correlation together with the nature of the

$\pi \rightarrow \pi^*$ transition provides insight into (1) why the first excitation energies calculated for the conjugated isoindole dimers are generally lower than those for the isoindole monomers, (2) why the first excitation energies calculated for both the monomer and dimer all become lower when R′ changes from H/CH_3 to CHO/C_6H_5, and (3) why the alternation of the nonconjugated substituents does not significantly change the calculated excitation energies. We note that the linear relationship (1) is valid only for one-electron excitations.

Our TD-DFT results indicate that the isoindole monomer structure **10a** itself does not have an absorption in the visible region ($\lambda >$ ~400 nm and $<$ ~700 nm),[50] whereas the dimer structures all have absorptions in the visible region. On the basis of our TD-DFT calculations of the **3b**, **6b**, and **8b** structures, the color of the light (~490 nm) absorbed by the direct products for the reactions of **1a** with amino acids/proteins under neutral and acidic conditions should be close to blue (~470 nm). The corresponding color of the nonabsorbed light should be close to orange, rather than the observed blue-violet color. This suggests that the blue-violet color is not due to the direct products of the possible dimerization of the isoindole structures.

Furthermore, we considered possible further oxidization of the formed isoindole monomer and dimer structures. Previously reported experimental studies[53] reveal that the methyl groups on the pyrrole ring in pyrrole-containing molecules are very unstable and could easily be oxidized into CHO. Thus, we examined model structure **11a** of the possible further oxidized isoindole monomer and model structures **5b** and **7b** of the possible further oxidized isoindole derivative dimer. On the basis of our TD-DFT results, the possible oxidization of the methyl group into CHO significantly decreases the excitation energies for both the monomer and dimer. However, the oxidized monomer structure (**11a**) still has no absorption in the visible region that can be expected to give a blue or violet color of the nonabsorbed light. The further oxidized dimer structures **5b** and **7b** have the strongest absorption at ~590 nm, which is between yellow (~580 nm) and orange (~620 nm). The corresponding color of the nonabsorbed light should be close to violet and blue, which is in good agreement with the observed violet/blue color of the products for the reactions of **1a** with amino acids/proteins under acidic condition.[9] So, the chromophores giving violet/blue color could be due to further oxidized isoindole derivative dimer structures such as **5b** and **7b**.

Compared to the model compounds **5b** and **7b**, the actual structure of the further oxidized isoindole derivative dimer formed from the reaction of **1a** with amino acids (such as lysine) or proteins differs in R where R is such that R−NH_3^+ represents an amino acid, polypeptide, or protein. In the case of proteins, the dimerization of the formed isoindole−protein adducts leads to cross-linking between the two proteins. This explains the experimental observation[9] that the γ-diketones, such as **1a**, cross-link neurofilament proteins to form higher-molecular-weight products. The cross-linked neurofilaments are unable to move anterogradely along the axon and, therefore, neurofilament transport is blocked. Our results strongly support the conclusion that the chromogenic effects of γ-diketones are closely related to their neurotoxic effects.[9] We further predict that both the chromogenic and neurotoxic effects are likely associated with the same reaction process, which probably starts from the formation of the isoindole−protein adducts followed by the dimerization and further oxidization. The previously examined possible ninhydrin-like reactions[8] lead to the colored products that do not cross-link proteins and, therefore, are not involved in the neurotoxic mechanism.

Possible Reaction Products under Basic Condition. The product structures formed under acidic conditions for the reactions of **1a** and **2a** with NH_3, in light of our estimated pK_a value, are dominated by their protonated/cationic states (like **3b**/**5b** and **4b**). The products formed under basic conditions should be dominated by their deprotonated/neutral states (like **3a**/**5a** and **4a**). As shown in Table 2, the excitation energies predicted for the neutral structures **5a** (formed from the further oxidization of the methyl groups) and **4a** are systematically higher (i.e., the wavelengths are systematically shorter) than the corresponding cationic structures. This suggests a possible pH dependence of the color of the products, consistent with the reported experimental results.[40] The reaction of **2a** with NH_3 produced a blue color in the presence of acid, whereas it produced a red color in the absence of acid. The blue and red chromophores are thought to be **4b** and **4a**, respectively.[40] As seen in Table 2, our TD-DFT calculation on **4a** predicts a strong absorption at ~521 nm, which is very close to the wavelength of green light (~530 nm). When green light is absorbed, the corresponding color of the nonabsorbed light is red. Our calculated results are consistent with the experimental observation.

As described in the literature,[9] the reactions of **1a** with amino acids/proteins also produce different colors under different conditions: the products formed under neutral and acidic conditions display a violet/blue color, whereas those formed under basic condition (when pH $\geq$ 7.5) display a brown color. This pH dependence of the color cannot be attributed to the ninhydrin-like reactions that are expected to always produce a blue color under neutral and basic conditions.[8] Whereas the violet/blue chromophores formed under neutral and acidic conditions can be assigned to be the oxidized isoindole derivative dimer structures such as **7b** on the basis of our TD-DFT calculations as noted above, it is interesting to note that the neutral oxidized dimer structure **7a** is predicted to have a very strong absorption at ~507 nm between blue (~470 nm) and green (~530 nm). The corresponding color of the nonabsorbed light should be between orange and red for **7a**, which is in agreement with the observed brown color of the products formed when pH $\geq$ 7.5. However, the structural assignment of the brown chromophore formed under basic condition is more complicated because the reaction mechanism for producing a structure like **7a** is not clear in the absence of further experimental studies. In contrast to the products of the reactions with NH_3 (or NH_4^+ for which R = H), as the possible products of the reactions with amino acids/proteins (for which R $\neq$ H) the cationic oxidized dimer structure **7b** cannot simply be transformed into the corresponding neutral oxidized dimer structure **7a** via deprotonation. If the brown chromophore formed under basic condition is really the oxidized dimer structure like **7a**, it only means that there are two possible competing reaction pathways for the reactions of **1a** with amino acids/proteins. One pathway leads to the oxidized dimer structure like **7b** cross-linking proteins, and the other leads to the oxidized dimer structure like **7a** without cross-linking proteins. The relative rates of the two reactions are dependent on the pH of the solution. The former is favored under neutral and acidic conditions, whereas the latter is favored when pH $\geq$ 7.5. However, the color of the products, once formed, is not expected to change rapidly by changing the pH of the solution.

Conclusion

We have performed a series of first-principles electronic structure calculations to predict the chromogenic properties of

various candidate structures, i.e., isoindole monomers and dimers and their derivatives, of the chromophores formed from the reactions of 1,2-diacetylbenzene (1,2-DAB), a typical representative of neurotoxic aromatic γ-diketones, with NH_3, amino acids, and proteins. The calculated results predict that the isoindole monomer structures do not have an absorption in the visible region ($\lambda > \sim$400 nm and $< \sim$700 nm), whereas the isoindole dimer derivatives all have absorptions in the visible region. The predicted electronic absorptions also show that oxidization of the methyl groups for the isoindole derivative dimers can significantly change the colors of the dimers. The calculated results for the oxidized isoindole derivative dimers are completely consistent with all of the experimental data linking the chromogenic and neurotoxic effects of 1,2-DAB. On the basis of comparison of the calculated results with the available experimental data, the violet/blue chromophores formed from the reactions of 1,2-DAB with amino acids/proteins under neutral and acidic conditions are likely to be the oxidized isoindole derivative dimer structures, e.g., **7b**, cross-linking the proteins, whereas the brown chromophores formed when pH $\geq$ 7.5 could be the oxidized dimer structures such as **7a** without cross-linking. Our results support the conclusion that the chromogenic effects of aromatic γ-diketones are closely related to their neurotoxic effects. Both the chromogenic and neurotoxic mechanisms are likely associated with the same reaction process, including the formation of the isoindole−protein adducts followed by the dimerization and further oxidization under neutral and acidic conditions. The possible existence of the oxidized derivative dimer structures such as **7a** in basic media should be examined in future experimental studies.

Acknowledgment. This research was performed in the William R. Wiley Environmental Molecular Sciences Laboratory (EMSL) at the PNNL. The EMSL is a national user facility funded by the Office of Biological and Environmental Research in the U.S. Department of Energy. PNNL is a multiprogram national laboratory operated by Battelle Memorial Institute for the U.S. Department of Energy. The work was funded in part by a subcontract from Oregon Health Sciences University under the auspices of a National Institute of Environmental Health Sciences Superfund Basic Research Center grant #5 P42 ES 10338.

Supporting Information Available: Geometries of **3a**, **3b**, **4a**, **4b**, **5a**, **5b**, **6a**, **6b**, **7a**, **7b**, **8b**, **9a**, **10a**, and **11a** optimized at the B3LYP/6-31+G(d) level. This material is available free of charge via the Internet at http://pubs.acs.org.

References and Notes

(1) Johnson, B. L.; DeRosa, C. T. *Rev. Environ. Health* **1997**, *12*, 235.
(2) Spencer, P. S.; Sterman, A. B.; Horoupian, D. S.; Folds, M. N. *Science* **1979**, *204*, 633.
(3) Spencer, P. S.; Folds, M. N.; Sterman, A. B.; Horoupian, D. S. In *Experimental and Clinical Neurotoxicology*; Spencer, P. S., Schaumburg, H. H., Eds.; Williams and Wilkins: Baltimore, 1980; p 296.
(4) Gagnaire, F.; Marignac, B.; de Ceaurriz, J. *J. Appl. Toxicol.* **1990**, *10*, 105.
(5) Gagnaire, F.; Ensminger, A.; Marignac, B.; de Ceaurriz, J. *J. Appl. Toxicol.* **1991**, *11*, 261.
(6) Spencer, P. S. In *Experimental and Clinical Neurotoxicology*, 2nd ed.; Spencer, P. S., Schaumburg, H. H., Eds.; Oxford University Press: New York, 2000; p 112.
(7) Kim, M.-S.; Sabri, M. I.; Miller, V. H.; Kayton, R. J.; Dixon, D. A.; Spencer, P. S. *Toxicol. Appl. Pharmacol.* **2001**, *177*, 121.
(8) Zhan, C.-G.; Dixon, D. A.; Sabri, M. I.; Kim, M.-S.; Spencer, P. S. *J. Am. Chem. Soc.* **2002**, *124*, 2744.
(9) Kim, M.-S.; Spencer, P. S.; Sabri, M. I. *Toxicol. Appl. Pharmacol.*, submitted for publication.
(10) Kim, M..S.; Kayton, R., Muñiz, J.; Austin, D. R.; Spencer; P. S.; Sabri, M. *Microsc. Microanal.* **1999**, *5* (Suppl. 2), 1218.
(11) DeCaprio, A. P. In *Experimental and Clinical Neurotoxicology*, 2nd ed.; Spencer, P. S., Schaumburg, H. H., Eds.; Oxford University Press: New York, 2000; p 633.
(12) Roberts, J. D.; Caserio, M. C. *Basic Principles of Organic Chemistry*; Benjamin: New York, 1965; p 708.
(13) Hohenberg, P.; Kohn, W. *Phys. Rev. B* **1964**, *136*, 864.
(14) Kohn, W.; Sham, L. J. *Phys. Rev. A* **1965**, *140*, 1133.
(15) Parr, R. G.; Yang W. *Density-Functional Theory of Atoms and Molecules*; Oxford University Press: Oxford, U.K., 1989.
(16) *Recent Advances in Density Functional Methods, Part 1*; Chong, D. P., Ed.; World Scientific: Singapore, 1995.
(17) Ando, T. *Z. Phys. B* **1977**, *26*, 263.
(18) Zangwill, A.; Soven, P. *Phys. Rev. A* **1980**, *21*, 1561.
(19) Runge, E.; Gross, E. K. U. *Phys. Rev. Lett.* **1984**, *52*, 997.
(20) Bauernschmitt, R.; Ahlrichs, R. *Chem. Phys. Lett.* **1996**, *256*, 454.
(21) Casida, M. E.; Jamorski, C.; Casida, K. C.; Salahub, D. R. *J. Chem. Phys.* **1998**, *108*, 4439.
(22) Casida, M. E.; Salahub, D. R. *J. Chem. Phys.* **2000**, *113*, 8918.
(23) (a) Matsuzawa, N. N.; Ishitani, A.; Dixon, D. A.; Uda, T. *J. Phys. Chem. A* **2001**, *105*, 4953. (b) Dixon, D. A.; Matsuzawa, N. N.; Ishitani, A.; Uda, T. *Phys. Stat. Sol.* **2001**, *226*, 69.
(24) Adamo, C.; Barone, V. *Chem. Phys. Lett.* **2000**, *330*, 152.
(25) (a) Zhan, C.-G.; Bentley, J.; Chipman, D. M. *J. Chem. Phys.* **1998**, *108*, 177. (b) Zhan, C.-G.; Chipman, D. M. *J. Chem. Phys.* **1998**, *109*, 10543. (c) Zhan, C.-G.; Chipman, D. M. *J. Chem. Phys.* **1999**, *110*, 1611. (d) Zhan, C.-G.; Landry, D. W.; Ornstein, R. L. *J. Phys. Chem. A* **2000**, *104*, 7672.
(26) (a) Becke, A. D. *J. Chem. Phys.* **1993**, *98*, 5648. (b) Lee, C.; Yang, W.; Parr, R. G. *Phys. Rev. B* **1988**, *37*, 785. (c) Stephens, P. J.; Devlin, F. J.; Chabalowski, C. F.; Frisch, M. J. *J. Phys. Chem.* **1994**, *98*, 11623.
(27) Hehre, W. J.; Radom, L.; Schleyer, P. v. R.; Pople, J. A. *Ab Initio Molecular Orbital Theory*; John Wiley & Sons: New York, 1986.
(28) Stratmann, R. E.; Scuseria, G. E.; Frisch, M. J. *J. Chem. Phys.* **1998**, *109*, 8218.
(29) Kaufmann, T. H.; Baumeister, W.; Jungen, M. *J. Phys. B* **1989**, *22*, 2223.
(30) Wan, J.; Meller, J.; Hada, M.; Ehara, M.; Nakatsuji, H. *J. Chem. Phys.* **2000**, *113*, 7853 and references therein.
(31) Kendall, R. A.; Dunning, T. H., Jr.; Harrison, R. J. *J. Chem. Phys.* **1992**, *96*, 6796.
(32) Schmidt, M. W.; Baldridge, K. K.; Boatz, J. A.; Elbert, S. T.; Gordon, M. S.; Jensen, J. H.; Koseki, S.; Matsunaga, N.; Nguyen, K. A.; Su, S. J.; Windus, T. L.; Dupuis, M.; Montgomery, J. A. *J. Comput. Chem.* **1993**, *14*, 1347.
(33) (a) Zhan, C.-G.; Norberto de Souza, O.; Rittenhouse, R.; Ornstein, R. L. *J. Am. Chem. Soc.* **1999**, *121*, 7279. (b) Zhan, C.-G.; Niu, S.; Ornstein, R. L. *J. Chem. Soc., Perkin Trans. 2* **2001**, *1*, 23. (c) Zheng, F.; Zhan, C.-G.; Ornstein, R. L. *J. Chem. Soc., Perkin Trans. 2* **2001**, 2355. (d) Zheng, F.; Zhan, C.-G.; Ornstein, R. L. *J. Phys. Chem. B* **2002**, *106*, 717.
(34) Zhan, C.-G.; Landry, D. W.; Ornstein, R. L. *J. Am. Chem. Soc.* **2000**, *122*, 2621.
(35) Zhan, C.-G.; Landry, D. W. *J. Phys. Chem. A* **2001**, *105*, 1296.
(36) Zhan, C.-G.; Zheng, F. *J. Am. Chem. Soc.* **2001**, *123*, 2835.
(37) Zhan, C.-G.; Dixon, D. A. *J. Phys. Chem. A* **2001**, *105*, 11534.
(38) (a) Zhan, C.-G.; Dixon, D. A. *J. Phys. Chem. A* **2002**, *106*, 9737. (b) Dixon, D. A.; Feller, D.; Zhan, C.-G.; Francisco, S. F. *J. Phys. Chem. A* **2002**, *106*, 3191. (c) Dixon, D. A.; Feller, D.; Zhan, C.-G.; Francisco, S. F. *Int. J. Mass Spectrom.*, in press.
(39) Frisch, M. J.; Trucks, G. W.; Schlegel, H. B.; Scuseria, G. E.; Robb, M. A.; Cheeseman, J. R.; Zakrzewski, V. G.; Montgomery, J. A.; Stratmann, R. E.; Burant, J. C.; Dapprich, S.; Millam, J. M.; Daniels, A. D.; Kudin, K. N.; Strain, M. C.; Farkas, O.; Tomasi, J.; Barone, V.; Cossi, M.; Cammi, R.; Mennucci, B.; Pomelli, C.; Adamo, C.; Clifford, S.; Ochterski, J.; Petersson, G. A.; Ayala, P. Y.; Cui, Q.; Morokuma, K.; Malick, D. K.; Rabuck, A. D.; Raghavachari, K.; Foresman, J. B.; Cioslowski, J.; Ortiz, J. V.; Stefanov, B. B.; Liu, G.; Liashenko, A.; Piskorz, P.; Komaromi, I.; Gomperts, R.; Martin, R. L.; Fox, D. J.; Keith, T.; Al-Laham, M. A.; Peng, C. Y.; Nanayakkara, A.; Gonzalez, C.; Challacombe, M.; Gill, P. M. W.; Johnson, B.; Chen, W.; Wong, M. W.; Andres, J. L.; Gonzalez, A. C.; Head-Gordon, M.; Replogle, E. S.; Pople, J. A. *Gaussian 98*, revision A.6; Gaussian, Inc.: Pittsburgh, PA, 1998.
(40) (a) Maekawa, E.; Suzuki, Y.; Sugiyama, S. *Chem. Ber.* **1968**, *101*, 847. (b) Nan'Ya, S.; Maekawa, E. *J. Chem. Soc. Jpn.* **1972**, 770. (c) Nan'Ya, S.; Maekawa, E. *J. Chem. Soc. Jpn.* **1974**, 1953. (d) Nan'Ya, S.; Maekawa, E. *J. Chem. Soc. Jpn.* **1975**, 1535.
(41) Chase, M. W., Jr. NIST-JANAF Tables, 4th ed. *J. Phys. Chem. Ref. Data* **1998**, Monograph 9, Suppl. 1.
(42) Tawa, G. J.; Topol, I. A.; Burt, S. K.; Caldwell, R. A.; Rashin, A. A. *J. Chem. Phys.* **1998**, *109*, 4852.
(43) Friedman, H. L.; Krishnan, V. V. *Water: A comprehensive treatise*; Plenum: New York, 1973.

(44) Tissandier, M. D.; Cowen, K. A.; Feng, W. Y.; Gundlach, E.; Cohen, M. H.; Earhart, A. D.; Coe, J. V. *J. Phys. Chem. A* **1998**, *102*, 7787.

(45) Mallard, W. G., Linstrom, P. J., Eds. NIST Chemistry WebBook. NIST Standard Reference Database Number 69, February 2000; National Institute of Standards and Technology: Gaithersburg, MD, 2000 (http://webbook.nist.gov).

(46) (a) Ruscic, B.; Feller, D.; Dixon, D. A.; Peterson, K. A.; Harding, L. B.; Asher, R. L.; Wagner, A. F. *J. Phys. Chem. A* **2001**, *105*, 1. (b) Ruscic, B.; Wagner, A. F.; Harding, L. B.; Asher, R. L.; Feller, D.; Dixon, D. A.; Peterson, K. A.; Song, Y.; Qian, X.; Ng, C.-Y.; Liu, J.; Chen, W.; Schwenke, D. W. *J. Phys. Chem. A* **2002**, *106*, 2727.

(47) (a) Wiberg, K. B.; Castejon, H.; Keith, T. A. *J. Comput. Chem.* **1996**, *17*, 185. (b) Merrill, G. N.; Kass, S. R. *J. Phys. Chem.* **1996**, *100*, 17465.

(48) McDouall, J. J.; Peasley, K.; Robb, M. A. *Chem. Phys. Lett.* **1988**, *148*, 183.

(49) Zhan, C.-G.; Dixon, D. A. *J. Mol. Spectrosc.* **2002**, *216*, 81.

(50) Atkins, P. W. *Physical Chemistry*, 3rd ed.; Oxford University Press: New York, 1988; p 432.

(51) Kotz, J. C.; Purcell, K. F. *Chemistry & Chemical Reactivity*; CBS College Publishing: New York, 1987; p 977.

(52) (a) Zhan, C.-G.; Nichols, J. A.; Dixon, D. A. *J. Phys. Chem. A*, submitted for publication. (b) Garza, J.; Fahlstrom, C. A.; Vargas, R.; Nichols, J. A.; Dixon, D. A. In *Reviews in Modern Quanum Chemistry: A Celebration of the Contributions of R. G. Parr*; Sen, K. D., Ed.; World Scientific: Singapore, 2003, p 1508. (c) Garza, J.; Vargas, R.; Nichols, J. A.; Dixon, D. A. *J. Chem. Phys.* **2001**, *114*, 639.

(53) Xu, G.; Singh, M. P.; Gopal, D.; Sayre, L. M. *Chem. Res. Toxicol.* **2001**, *14*, 264.